Applied Catalysis A: General 374 (2010) 180–188

Pd-In_2O_3 Interaction due to Reduction in Hydrogen: Consequences for Methanol Steam Reforming

H. Lorenz[1], S. Turner[2], O. I. Lebedev[2], G. Van Tendeloo[2], B. Klötzer[1], C. Rameshan[1,3], K. Pfaller[4], S. Penner[1,*]

[1]Institute of Physical Chemistry, University of Innsbruck, A-6020 Innsbruck, Austria
[2]EMAT, University of Antwerp, B-2020 Antwerp, Belgium
[3]Department of Inorganic Chemistry, Fritz-Haber Institute of the Max-Planck Society, D-14195, Berlin, Germany
[4]Section of Histology and Embryology, Medical University Innsbruck, A-6020 Innsbruck

[*] Corresponding author: e-mail simon.penner@uibk.ac.at,

Received: 24 September 2009; Received in revised form 2 December 2009; Accepted 3 December 2009
Available online 24 December 2009

Abstract

Two different Pd/In_2O_3 samples including a thin film model catalyst with well-defined Pd particles grown on NaCl(001) supports and a powder catalyst prepared by an impregnation technique are examined by Electron Microscopy, X-ray Diffraction and catalytic measurements in methanol steam reforming in order to correlate the formation of different oxide-supported bimetallic Pd-In phases with catalytic activity and selectivity.

A PdIn shell around the Pd particles is observed on the thin film catalyst after embedding the Pd particles in In_2O_3 at 300 K, likely because alloying to PdIn and oxidation to In_2O_3 are competing processes. Increased PdIn bimetallic formation is observed up to 573 K reduction temperature until at 623 K the film stability limit in hydrogen is reached. Oxidative treatments at 573 K lead to decomposition of PdIn and to the formation of an In_2O_3 shell covering the Pd particles, which irreversibly changes the activity and selectivity pattern to clean In_2O_3.

PdIn and Pd_2In_3 phases are obtained on the powder catalyst after reduction at 573 K and 673 K, respectively. Only CO_2-selective methanol steam reforming is observed in the reduction temperature range between 473 K and 573 K. After reduction at 673 K encapsulation of the bimetallic particles by crystalline In_2O_3 suppresses CO_2 formation and only activity and selectivity of clean In_2O_3 are measured.

Keywords: Electron Microscopy; Pd-In intermetallics; PdIn; Pd_2In_3; methanol steam reforming

1. Introduction

Pd-In bimetallic compounds are primarily known to promote the catalytic hydrogenation of nitrates or the reduction of NO by CO [1,2]. Another aspect is their potential catalytic function in methanol steam reforming, thus opening a selective reaction pathway to H_2 and CO_2 [3]. As in the latter case the bimetallic Pd-In phase(s) are prepared via reduction of Pd particles supported on In_2O_3, questions arise about the potential catalytic contribution of the supporting oxide. Particularly since it has been shown that the activity and selectivity of pure In_2O_3 has to be taken into account upon discussing catalytic properties of In_2O_3-supported Pd-In bimetallic phases [4]. In_2O_3 itself is a highly CO_2-selective methanol steam reforming catalyst at temperatures $T \geq 573$ K, which is usually interpreted in terms of its redox properties and its pronounced basic character, thus favouring complete oxidation of methanol [4,5]. As for the corresponding Pd-Ga system, an additional complication may arise from the rather complex Pd-In phase diagram, which exhibits a number of thermodynamically stable phases and may impose difficulties in preparing oxide-supported single bimetallic phases [6].

To tackle this problem and to structurally and catalytically characterize Pd-In bimetallic phases with defined stoichiometries, a combined approach via a thin film model concept and studies on the related powder catalysts will be followed. This strategy, which involves the preparation of

the Pd-In particles by reduction in hydrogen, has proven its capabilities in studies on the corresponding Pd-Ga system [7,8]. On the one hand the thin film model approach allows to prepare and characterize well-defined Pd-In bimetallic particles, grown on single-crystalline NaCl(001) surfaces, with respect to morphology, composition and catalytic selectivity. On the other hand correlations to more realistic catalyst systems can be easily established by studying reactivity and selectivity under identical conditions. The present contribution therefore aims at (i) an easy and reproducible preparation of Pd-In bimetallic particles supported on In_2O_3, (ii) a thorough structural characterization by electron microscopy and X-ray diffraction, and (iii) a catalytic characterization in methanol steam reforming. Special attention will also be paid to the influence of strong-metal support interaction effects (i.e. decoration of metal/bimetallic particles by oxide species upon reduction in hydrogen) on the catalytic activity/selectivity and a detailed comparison of the results with those of the related Pd-Zn and Pd-Ga systems. Despite their similar catalytic selectivity [4], due to the more easy reducibility of In_2O_3, differences in both bimetallic formation and catalytic behaviour are expected.

2. Experimental

A high-vacuum chamber (base pressure 10^{-4} Pa) was used to prepare the In_2O_3-supported Pd thin film model catalysts. For preparation of electron microscopy films, Pd metal was deposited by electron-beam evaporation onto a freshly-cleaved NaCl(001) plane at a base pressure of 10^{-4} Pa and a substrate temperature of 623 K (area of the NaCl single crystal about 0.25 cm^2). Subsequently, the Pd particles were covered by a layer of In_2O_3 (nominal thickness: 25nm), prepared by reactive deposition of In_2O_3 in 10^{-2} Pa O_2 at either 300 K or 600 K. As for the catalytic experiments in the micro-reactor larger-area samples are necessary to obtain sufficiently high conversion rates, thin films subsequently used for the catalytic experiments were prepared in parallel on freshly deposited polycrystalline NaCl thin films with larger surface area in a similar way as discussed above. The NaCl thin film supports were prepared by deposition of a polycrystalline NaCl thin film (thickness: 600 nm) at 298 K on two specially designed Cu sheets (37 cm^2 each). The structure of metal particles and support is almost identical on both substrates [9]. For subsequent structural characterization by electron microscopy, the resulting Pd/In_2O_3 films were floated into distilled water by dissolution of NaCl and rinsed with distilled water, dried and finally mounted on gold grids. All films used for catalytic measurements were additionally covered by a supporting layer of amorphous SiO_2, prepared by reactive deposition of SiO in 10^{-2} Pa O_2 at 298 K (mean SiO_2 film thickness: 1000 nm). The choice for SiO_2 as the strengthening layer was basically due to its easy evaporation/deposition and its inert chemical and catalytical nature. These films were subsequently floated in distilled water and thoroughly rinsed and dried before mounting on quartz wool inside the reactor.

The Pd/In_2O_3 powder catalyst was prepared via impregnation of In_2O_3 powder with small Pd particles. For this purpose, In_2O_3 powder (Alfa Aesar, 99.99%, BET surface area 1 m^2/g) was dispersed in ~150 ml distilled water and the Pd precursor ($Pd(NO_3)_2$ 99.95%, metals basis, 12 % Pd) was slowly added under permanent vigorous stirring. Finally, the water was evaporated and the resulting catalyst subjected to an oxidative treatment in air at 873 K for 1h. This procedure converts the catalyst into PdO/In_2O_3, as verified by routine X-ray diffraction measurements.

Reductive (1 bar H_2 for 1h), oxidative (1 bar O_2 for 1h) and tempering treatments in He (1 bar) were performed in parallel in a circulating batch reactor in the temperature range between 373-773 K. Structural and morphological changes were followed by (high-resolution) electron microscopy (HRTEM) and selected area electron diffraction (SAED). The electron micrographs were taken with a ZEISS EM 10C, a JEOL 4000EX electron microscope operated at 400 kV with a point resolution of 1.7Å and a FEI TECNAI G2 S-TWIN analytical (scanning-) transmission electron microscope operated at 200kV. High angle annular dark field scanning transmission electron microscopy (HAADF-STEM) images were obtained using an approximate detector with an inner semi-angle of 90 mrad. The film composition was checked by energy-dispersive X-ray spectroscopy (EDXS). Basically only peaks originating from the evaporated thin film constituents (Pd, In and O) and the gold grid (Au) were detected. The purity of the substrate was ensured by freshly cleaving the NaCl(001) crystals immediately before deposition of the oxide. The SAED patterns were calibrated with respect to the Pd reflections in the untreated, as-grown state of the catalyst.

X-ray diffraction experiments were performed ex-situ under ambient conditions using a Siemens D5000 Spectrometer and Cu-K_α radiation (1.54178 Å) at 300 K.

SEM experiments were conducted in an SM 982 GEMINI ZEISS field emission scanning electron microscope. Prior to SEM imaging, the samples were coated with 5 nm Au/Pd to improve its conductance and fixed with conducting carbon paste.

Catalytic measurements in methanol steam reforming as well as catalyst activation treatments of *all* samples were performed in an NI Labview-automatized recirculating batch reactor of about 8 ml volume [10]. The system allows automated pre-treatment cycles (oxidative and reductive) and reaction sequences. As the measurements should in principle allow assessing the contribution of different oxide-supported Pd-In bimetallics to the activity and selectivity in methanol steam reforming, activation treatments typically used for supported Pd catalysts to induce the formation of the potentially selective Pd-In bimetallics were chosen [3]. Standard activation treatments therefore include oxidation in 1 bar O_2 at 673 K followed by reduction in 1 bar H_2 at varying temperature. For thin films, reduction temperatures between 373 K and 623 K were usually ap-

plied. Pd/In_2O_3 powder samples were treated in hydrogen at temperatures as high as 773 K.

The catalytic measurements were performed using a quadrupole mass spectrometer (Balzers QMG 311) attached to the circulating batch Duran glass reactor via a capillary leak. All methanol steam reforming reactions were conducted with methanol/water mixtures of a 1:9 composition of the liquid phase at room temperature. The gas phase compositions of a variety of different liquid mixtures have been empirically determined by mass spectrometry. On the basis of these measurements we could derive that the volumetric 1:9 mixture corresponds to a gas phase composition of 1:2 = methanol:water at room temperature. All methanol/water mixtures were degassed by repeated freeze-and-thaw cycles. For each catalytic methanol steam reforming experiment, to about 50 mbar methanol/water mixture, 7.5 mbar Ar (to be measured at m/z = 40) was added to account for the decrease of the mass spectrometer signal due to the continuous gas withdrawal through the leak. Finally, He was added to 1 bar total pressure.

The molecular masses m/z =2 (H_2), 16 (CH_4), 18 (H_2O), 28 (CO/N_2), 29 ($CH_3OH/HCOOH$), 30 (CH_2O), 31 (CH_3OH/CH_2O), 32 (CH_3OH/O_2), 40 (Ar) and 44 (CO_2), 45 (HCOOH) and 46 (HCOOH) were routinely collected. All mass spectrometer signals of CH_3OH, CO_2 and CO were externally calibrated and corrected for fragmentation in the mass spectrometer. This includes m/z = 28 for both CO_2 and CH_3OH and m/z = 45 for CO_2. The mass m/z = 28 is therefore only influenced by CH_3OH, CO_2, and the formed CO via the reaction itself. In order to account for the partial adsorption of methanol and water on the stainless steel parts of the reaction system, all catalytic measurements include a 15 minute equilibration period in the starting mixture prior to each measurement. For methanol steam reforming, both temperature-programmed conversion and conversion versus time under isothermal conditions were monitored. In each case, the catalyst was exposed to the reaction mixture and the temperature was ramped with 5 K/min to the final value. For the partial pressure change versus time experiments, the product formation was monitored for 1 hour each at fixed reaction temperature. All the catalytic experiments were also corrected for the activity of the catalyst holder containing only quartz wool (almost negligible, at maximum 1 % conversion based on CO_2 formation after 1 h). For data evaluation, the relative intensities of the mass spectrometer signals were converted into partial pressures via external calibration using gas mixtures of defined partial pressures.

For clarity, all catalytic results are usually plotted as partial pressure change versus temperature or time. The initial slopes of the conversion versus time plots were taken to determine (initial) reaction rates and turnover frequencies (TOF, molecules per site and hour). Details of the determination of the TOF are given in section 3.2.

3. Results

3.1. Structural characterization

3.1.1. The as-prepared state

The first differences to the as-prepared state of the Pd-ZnO and Pd-Ga_2O_3 thin film model catalysts [7,11] are noticed in Figure 1, highlighting the initial, untreated Pd/In_2O_3 film. The bright-field TEM image of Fig. 1a already highlights the major difficulty in structurally characterizing all Pd/In_2O_3 thin film catalysts. The In_2O_3 support exhibits a network of inter-connected round-shaped grains (average size: 5-10 nm) with strong contrast variations, mostly due to diffraction contrast of differently oriented In_2O_3 grains [12]. In contrast to Pd on amorphous ZnO or Ga_2O_3, the Pd particles are not easily detected in these bright-field TEM images. A combination of dark-field and high-angle annular dark-field imaging was used to locate the Pd particles. Figure 1b shows a dark field image using the combined (200), (-200), (020) and (0-20) Pd diffraction spots (see Figure 1c). The image is a superposition of four individual dark field images taken with each of the four diffraction spots; all the very bright dots indicate Pd particles. Due to the finite size of the aperture, small contributions from In_2O_3 diffraction spots are inevitable, giving rise to the grey background in the image. These observations are corroborated by additional HAADF images (Figure 1d). Since the HAADF contrast, constant thickness and density provided, is approximately proportional to $Z^{1.5\text{-}2}$ (Z denoting the average atom number), regions with higher average Z will appear brighter. Hence in the case of Pd/In_2O_3, the Pd particles will appear brighter than the In_2O_3 support (average Z of Pd is 46, average Z of In_2O_3 is 24.4). The Pd particles appear to be evenly distributed with sizes around 5-10 nm.

The corresponding SAED patterns (Figure 1c) reveal epitaxially grown Pd particles with strong (200) [at d~1.94Å] and (220) [at d~1.37Å] diffraction spots, arising from Pd (fcc crystal structure) particles oriented along the [001] zone axis. In other patterns also randomly arranged diffractions spots of the bcc In_2O_3 can be detected. The most intense reflection of the bcc In_2O_3 structure is a rather broad Debye-Scherrer-type ring reflection at around 2.9Å, corresponding to the (222) lattice spacing [13]. Additional, rather faint reflections, which cannot be assigned to either Pd metal or In_2O_3 are observed at d~2.28Å (less clearly because of overlap with the Pd(111) and In_2O_3(420) reflections [d_{theor}Pd(111)=2.245Å and $d_{theor}In_2O_3$(420)=2.265Å]), d~1.6Å, and ~1.32Å. Although In_2O_3 was deposited at 300 K, we tentatively address these reflections to the (110), (200) and (211) lattice spacing of the simple cubic PdIn bimetallic phase (lattice constant a=3.249Å; d_{theor}PdIn(110)=2.297Å, d_{theor}PdIn(200)=1.624Å, d_{theor}PdIn(211)=1.326Å) [14]. Since these spots are well-aligned with respect to the fcc Pd reflections, the growth of this compound seems to be mediated by the structure of Pd.

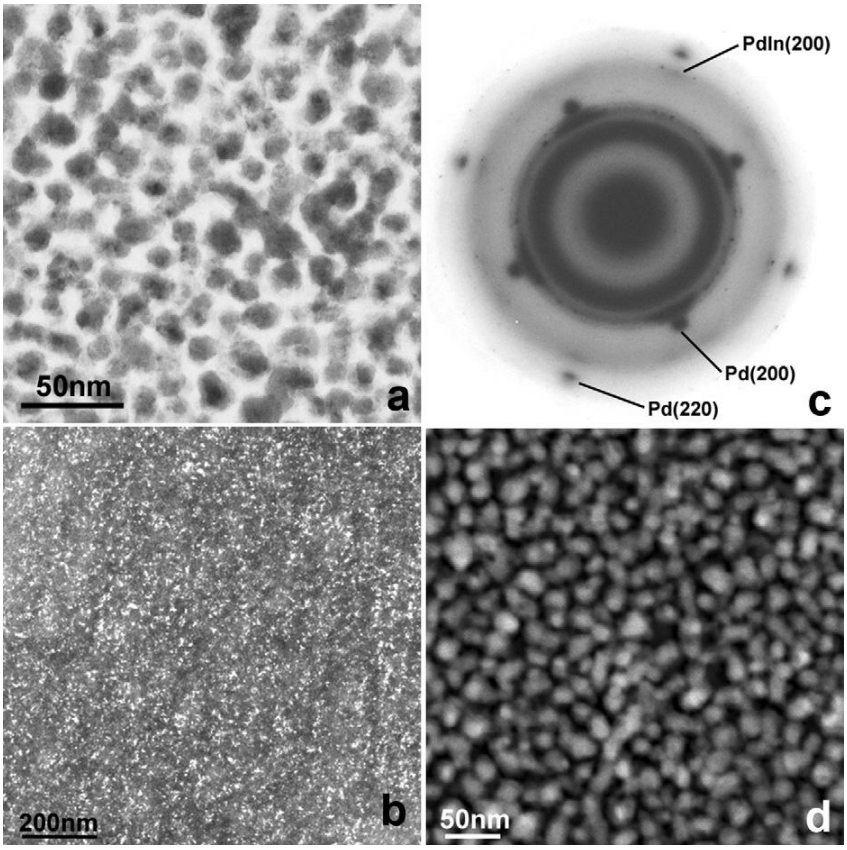

Fig. 1: Bright-field overview TEM image of the as-deposited Pd/In_2O_3 thin film catalyst (a), dark field image (b), corresponding SAED pattern (c) and HAADF-STEM image (d) of the as-grown state of the Pd-In_2O_3 thin film catalyst.

A similar observation has been made for a Pd/In_2O_3 thin film catalyst with higher Pd loading. Since for pure In_2O_3 partially crystalline films are only obtained at low substrate temperatures (300 K), and since only at higher substrate temperatures full oxidation and crystallization to In_2O_3 is observed, we conclude that the bimetallic formation at T = 300 K is a result of the dominating alloying process over the slower re-oxidation of sub-stoichiometric In-oxides and In metal to In_2O_3 during the deposition process. Our observations agree well with studies of Veltruska et al. [15], who studied the Pd-In interaction during Pd deposition on In_2O_3 films. Pd-In alloy formation was observed and verified by XPS and LEIS if Pd is deposited on a partially reduced (i.e. sputtered) In_2O_3 support at 300 K. For our samples, evidence for bimetallic formation at 300 K is also obtained by a strong intensity increase of the PdIn diffraction spots ((110, (200) and (211)) upon hydrogen reduction at temperatures as low as 373 K. This is at much lower temperatures than expected from previous experiments on Pd/ZnO and Pd/Ga_2O_3 or by studies of Iwasa et al. [3]. Additional evidence comes from catalyst regeneration experiments in oxidizing environments and from catalytic measurements in methanol steam reforming as will be discussed later.

The question why bimetallic formation is observed on Pd/In_2O_3 thin film model catalysts already after deposition of In_2O_3 at 300 K - in contrast to Pd/ZnO and Pd/Ga_2O_3 - can be interpreted in terms of the high reducibility of In_2O_3 to metallic In during the deposition process. In_2O_3 is set apart from Ga_2O_3 (which only yields sub-stoichiometric oxides, predominantly Ga_2O, but no Ga metal), as it readily loses oxygen upon heating in a Ta crucible, forming a combination of sub-stoichiometric oxides *and* metallic In in the gas phase. Thus, despite deposition in 10^{-2} Pa oxygen, some metallic In and/or sub-oxidic remains, because the re-oxidation rate to In_2O_3 is limited around 300 K. Such species will in turn most probably form a thin shell of PdIn around the Pd particles. In general, formation of bulk Pd-In alloys has been observed to be a strongly exothermic process, proceeding already at low temperatures [16,17].

Figure 2 shows a representative TEM image of a Pd/In_2O_3 powder catalyst after reduction at 373 K. Pd particles with an average size of 3-10 nm are visible decorating a single round-shaped In_2O_3 grain. It should be noted that this configuration is very sensitive to the electron beam; rapid agglomeration of the Pd particles is frequently observed.

Nevertheless, for a better comparison with the studies on Pd/ZnO and Pd/Ga_2O_3, these two preparations of the catalysts will in the following serve as the structural reference for all changes occurring during catalyst activation treatments.

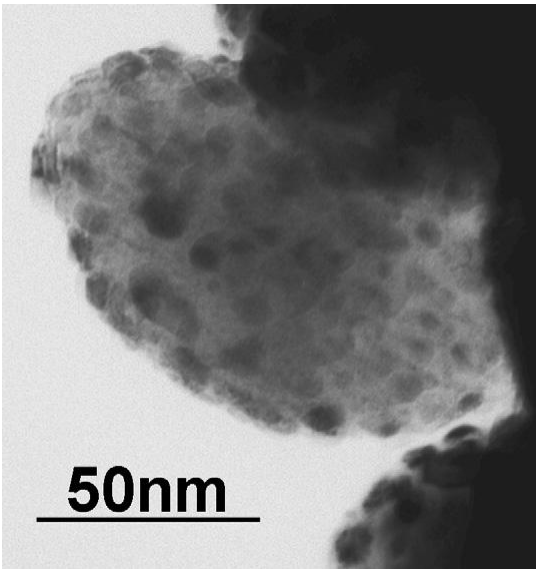

Fig. 2: TEM image of the Pd/In_2O_3 powder catalyst after reduction at 373 K

3.1.2. Bimetallic formation and stability

To correlate the present experiments to previous Pd-ZnO and Pd-Ga_2O_3 results [7,11], the Pd-In_2O_3 catalysts were subsequently subjected to reductive treatments in hydrogen at temperatures between 373 K and 623 K (without oxidation in between). Figure 3 shows the state of the thin film model catalyst after reduction in hydrogen at 373 and 473 K, respectively. In general, the detection of the Pd/PdIn particles is not straightforward (see Figures 3a and b). However, the SAED patterns indicate increased bimetallic formation at 373 K, as deduced from the intensity increase of especially the PdIn(200) reflection (Figure 3c). This is accompanied by a slight decrease of the Pd diffraction spot intensity. At 473 K, complete crystallization of In_2O_3 is evident in the SAED patterns (Figure 3d) and the Pd(200) spots have almost vanished. Accordingly, the intensity of the PdIn diffraction spots increased. Therefore, it is also clear that the intense four-fold split spots at ~ 2.3Å, formerly overlapping with the Pd(111) reflection, correspond to PdIn(110) [14]. From the alignment of the diffraction spots we conclude that PdIn mainly grows in the following epitaxial relation: PdIn[001]//Pd[001] and PdIn[011]//Pd[011]. Because of the high mobility of In_2O_3, the bright-field TEM images at 473 K also indicate a beginning reconstruction of the supporting film. Larger In_2O_3 grains and closing of grain boundaries are much more pronounced at 573 K, (Figure 4a). At this temperature, no metallic Pd is left according to the SAED patterns and the size of the bimetallic particles has very much increased. Since only Debye-Scherrer-type diffraction rings are observed (Figure 4b), the patterns also indicate a complete loss of azimuthal ordering of the PdIn particles. At this temperature the film stability limit in hydrogen is reached. Pure In_2O_3 films showed decomposition at $T \geq 673$ K, but the onset temperature is expected to be much lower in the presence of Pd (or PdIn) being capable of enhanced dissociative hydrogen adsorption.

In order to determine the possibility of catalyst regeneration, the oxidative stability of the PdIn bimetallic was tested. Therefore, the catalyst was pre-treated in hydrogen at 473 K and subsequently re-oxidized between 373 K and 673 K. The PdIn bimetallic proved to be stable below 473 K oxidation temperature, but beginning decomposition was observed at 473 K, where faint Pd(200) spots reappeared. At 573 K, PdIn fully decomposed, as indicated by the SAED pattern, which basically becomes a superposition of the patterns of fcc Pd and bcc In_2O_3 (Figure 4d). It is worth to note, that the particles retain their epitaxial relationship even after the reduction-oxidation cycle. More crucial, however, is the morphological transformation of the bimetallic particles. The TEM image of Figure 4c reveals small Pd particles centered on almost every In_2O_3 grain with a much enhanced contrast compared to the as-grown state (highlighted particles in Figure 4c). It is also worth noting that the same enhanced contrast can be obtained by simple oxidation of the as-grown state at 673 K. As outlined above, this contrast enhancement is in any case associated with the decomposition of PdIn, either causing the presence of clean Pd with a free and accessible metal area or the decomposition of the bimetallic leads to metallic Pd encapsulated with a shell of In_2O_3; this would be similar to what has been observed for Pd-Ga_2O_3 [11]. Since the particles on the thin film are imaged in plan view, identification of this core shell structure is not straightforward. Its presence though is further indirectly confirmed by the suppressed PdO formation and the altered catalytic properties. If the Pd particles get encapsulated by In_2O_3, the diffusion of oxygen to metallic Pd may become blocked, thus suppressing PdO formation. We also expect the catalytic activity/selectivity pattern of In_2O_3 to become dominant in case of encapsulation with suppressed methanol dehydrogenation if the free Pd metal area is blocked; this prediction will be treated in section 3.2. Figure 4d reveals that after oxidation at 573 K only metallic Pd is present. Even after oxidation at 673 K, where a full transformation of Pd into PdO has been observed on Pd/SiO_2 catalysts [18], only Pd metal without detectable PdO formation is found. A further indication towards the presence of an In_2O_3 shell arises from experiments of repeated reduction *after* oxidation at 673 K. If only Pd metal is present after oxidation, we would expect the onset of bimetallic formation at temperatures comparable to those for Pd-ZnO or Pd/Ga_2O_3 (473-523 K), or even at lower temperatures as indicated by Iwasa et al. [3] (bimetallic formation on Pd/In_2O_3 powder samples was induced by reduction at 523 K compared to at 773 K on Pd/ZnO or Pd/Ga_2O_3). Figure 5 reveals that after repeated reduction at temperatures of ~ 473 K no sign of PdIn bimetallic formation is present. The metallic particles still exhibit their enhanced contrast (Figure 5a) and the SAED pattern did not change compared to the state after oxidation at 673 K (Figure 5c). Bimetallic formation is only observed

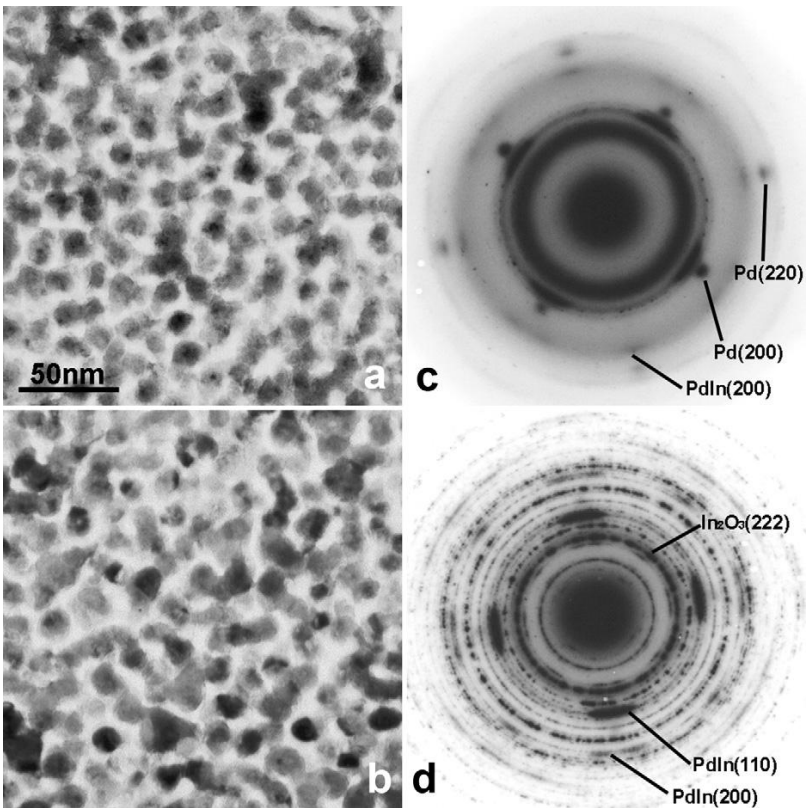

Fig. 3: TEM image of the Pd/In_2O_3 thin film catalyst after reduction at 373 K (a) and 473 K (b). The corresponding SAED patterns are shown in (c) and (d), respectively.

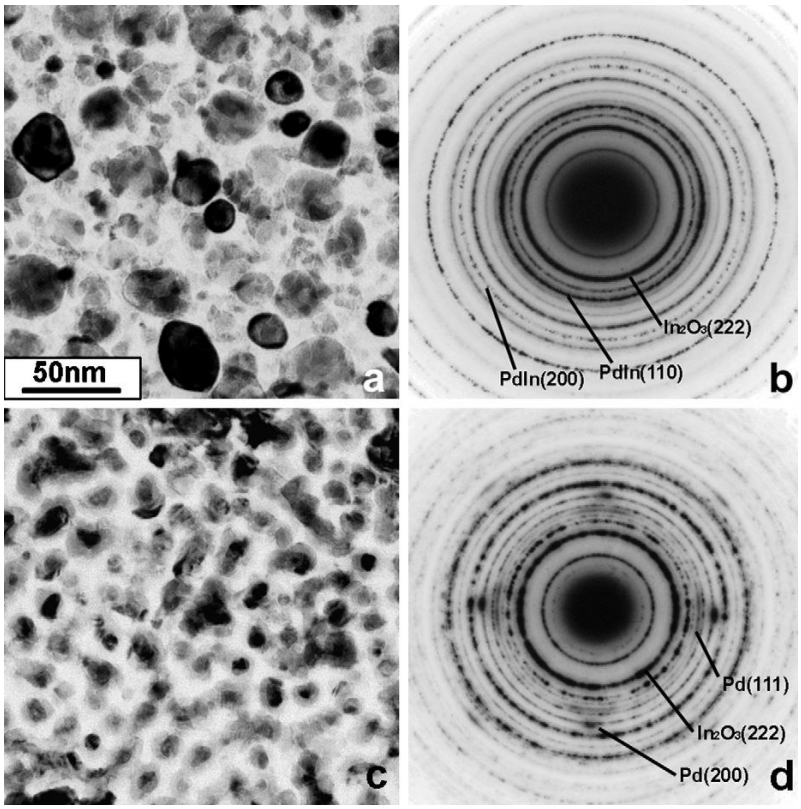

Fig. 4: TEM image of the Pd/In_2O_3 thin film catalyst after reduction at 573 K (a) and the corresponding SAED pattern (b). TEM image of the Pd/In_2O_3 thin film catalyst after reduction at 473 K followed by re-oxidation at 573 K (c). The corresponding SAED patterns are shown in (d).

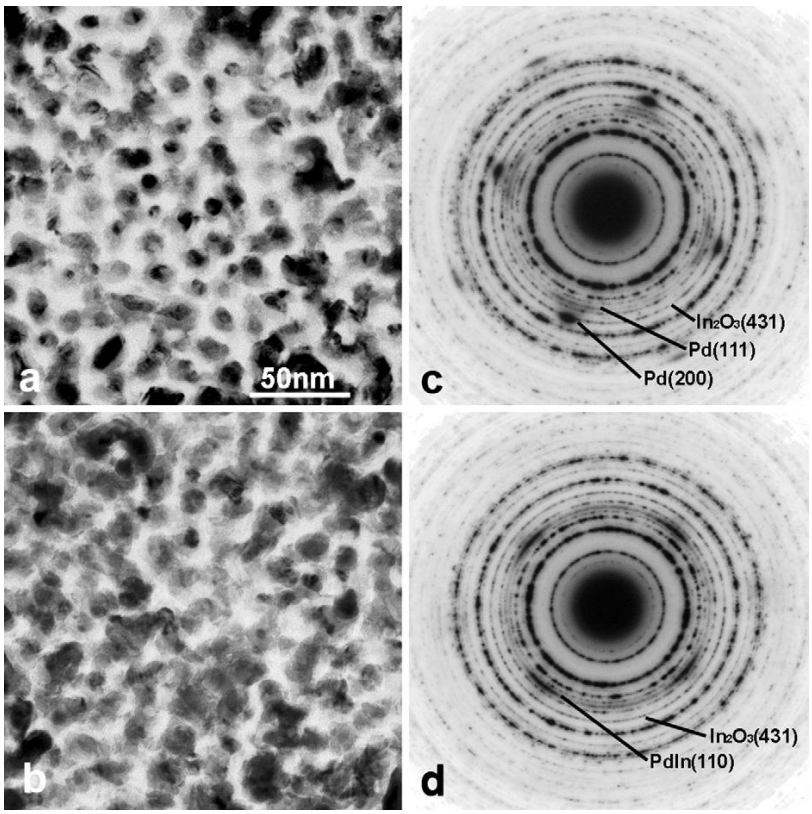

Fig. 5: TEM image of the Pd/In_2O_3 thin film catalyst after reduction at 473 K followed by re-oxidation at 673 K and re-reduction at 473 K (a) and 573 K (b). The corresponding SAED patterns are shown in (c) and (d), respectively.

after repeated reduction at 573 K, close to the decomposition temperature of the whole substance of the thin films. The enhanced contrast is lost (Figure 5b) and the SAED patterns show the presence of cubic PdIn and bcc In_2O_3 (Figure 5d). Although the effect of suppressed bimetallic formation is small, we conclude that the In_2O_3 shell is responsible for this shift in the onset temperature of PdIn formation by approximately 50 K.

The structural transitions of the Pd/In_2O_3 powder catalyst were followed by XRD and HRTEM. Figure 6 depicts a set of XRD spectra collected after different reductive treatments. Reduction between 300 K and 473 K causes formation of metallic Pd and bcc In_2O_3. At 573 K reduction temperature, bulk PdIn is formed and no metallic Pd persists. Reduction at 673 K causes the formation of an even more In-rich bimetallic, namely Pd_2In_3 (hexagonal lattice; a=4.52 Å; c=5.49 Å) [19]. Strong reflections in the XRD pattern include the (011), (110) and (012) peaks (d_{theor}=3.187 Å, d_{theor}=2.260 Å, d_{theor}=2.247 Å, respectively). Higher reduction temperatures (T > 673 K) result in a mixture of Pd_2In_3, $PdIn_3$ (bcc lattice, a=9.433Å; strongest reflection at 2.218Å [14]) and most probably In metal (overlapping with $PdIn_3$, tetragonal lattice; a=3.25Å, c=4.94Å [20]). As a result, it should in principle be possible to study the catalytic activity of two distinct oxide-supported Pd-In bimetallics, PdIn and Pd_2In_3. As will be corroborated by the catalytic measurements discussed below, (HR)TEM results indicate encapsulation of the (bi)metallic particles as a second manifestation of strong metal-support interaction at reduction temperatures 573-673 K, apart from bimetallic formation. Among the three investigated powder catalyst systems Pd-ZnO, Pd-Ga_2O_3 and Pd-In_2O_3, this was only detected for the latter. After reduction at 573 K, the bimetallic particle size has only increased modestly, but after reduction at 673 K, very large bimetallic particles have been observed with an average size about 10-25 nm (Figure 7 upper panel); an SEM image, giving an overview of the catalyst after reduction at 673 K is shown in the lower panel of Figure 7. Large sintered In_2O_3 grains are evenly decorated with small Pd_2In_3 particles. The porous structure of In_2O_3, which was not observed after reduction of the pure In_2O_3 powder at comparable reduction temperatures, appears to be due to the thorough reduction of the In_2O_3 in the presence of Pd and the associated high mobility, a prerequisite for SMSI-type behaviour.

HRTEM imaging reveals encapsulation of the bimetallic nanoparticles. Figure 8 shows a part of an In_2O_3 grain that is decorated with bimetallic nanoparticles smaller than 10 nm. Both particles are PdIn and are imaged close to the [111] zone axis orientation (note that XRD at this stage of reduction basically reveals the presence of a Pd_2In_3 bimetallic phase. However, we cannot exclude some PdIn formed at lower reduction temperatures still persisting, partly also due to the parallel formation of the oxide shell around the bimetallic particles). The orientation and crystal

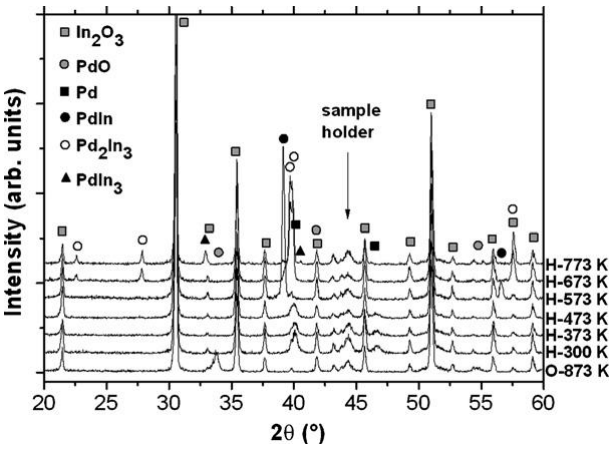

Fig. 6: Set of XRD spectra taken after reduction reduction stages of the Pd/In_2O_3 powder catalyst.

structure is evidenced for the bottom nanoparticle by the inset FFT pattern (inset figure 8). All reflections in the FFT pattern correspond to a 2.3Å d_{110} spacing. The black arrows in the HRTEM image indicate the encapsulation of the nanoparticles. A clear layer can be distinguished that covers the entire free surface of both nanoparticles. The surface layer is disordered/amorphous in most cases. TEM measurements show that fast crystallisation of the surface layer occurs under the electron beam forming thin layers (2-3 unit cells) with an approximate interspacing of 2.5Å, corresponding to the (400) lattice planes of the bcc In_2O_3 structure.

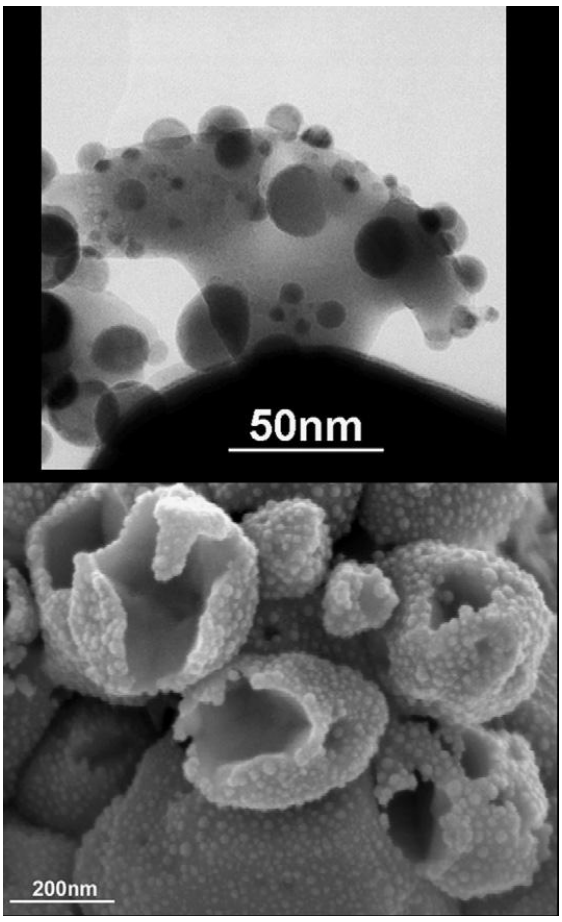

Fig. 7: TEM image of the Pd/In_2O_3 powder catalyst after reduction at 673 K (upper panel) and the corresponding SEM image (lower panel).

3.2. Catalytic characterization in methanol steam reforming

In the following, both the thin film and the powder Pd-In_2O_3 catalysts were subjected to different oxidative and reductive pre-treatments in order to assess the catalytic contribution of different Pd-In bimetallics and the SMSI shell to verify the different manifestations of metal-support interaction. Compared to Pd/ZnO and Pd/Ga_2O_3, however, the separation between the catalytic selectivity of the Pd-In bimetallic and the In_2O_3 support will be hampered by the pronounced CO_2-selectivity of pure In_2O_3 (> 95% [4]). Differences will hence most likely be noticed only in the onset temperature of methanol steam reforming, since it is expected that key reaction intermediates are formed and/or stabilized at lower temperature if free bimetallic area is available.

Figure 9 (left panel, a and c) shows the methanol steam reforming reaction over the Pd/In_2O_3 powder catalysts pre-reduced at 473, 573 and 673 K. Figure 9a highlights the H_2 and methanol (m/z = 31) traces, Figure 9c the CO_2 and CO traces. On the initial, as-prepared catalyst, methanol dehydrogenation is the pre-dominant reaction at low reaction temperatures giving rise to increased formation of CO (not shown). Only at higher reaction tempera tures (T > 623 K) contributions from In_2O_3, resulting in increased formation of CO_2, are also noticed (not shown here). After pre-reduction at 473 K, however, CO_2 formation starts at around 510 K and accelerates in the temperature range 510-670 K. CO formation remains suppressed over the entire reaction temperature range. The methanol traces decrease and the H_2 signals increase accordingly. Note that the H_2 traces exceed the sensitivity limit of the mass spectrometer at higher reaction temperatures (this is basically due to a mass spectrometer sensitivity compromise between the detection of CO/CO_2 and H_2). Although the XRD patterns show no signs of Pd-In bulk structures after 473 K reduction, the catalytic experiments strongly indicate the presence of a thin Pd-In bimetallic shell around the Pd particles. A significant contribution of free Pd metal area can be excluded since no substantial methanol dehydrogenation behaviour has been observed at low reaction temperatures, according to the results in Figure 9. In the temperature range 510-550 K, we also exclude a predominant contribution from the In_2O_3 support, since the onset temperature of the methanol steam reforming reaction over the pure support is around 550 K and a strong acceleration of the reaction is only observed at temperatures T > 600 K. After pre-reduction at 573 K, the onset temperature is still observed at around 510-520 K, but CO_2 formation occurs at

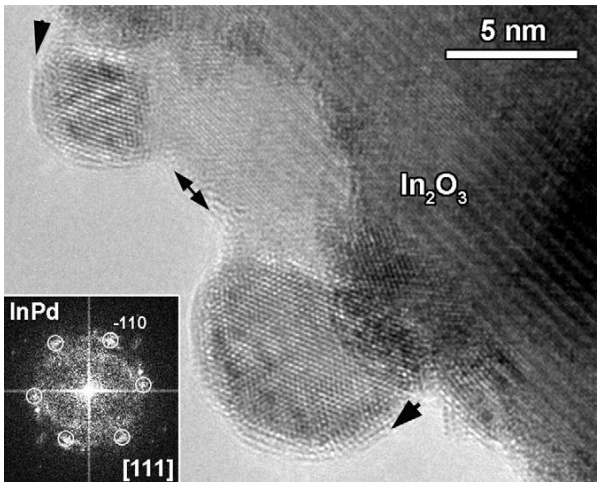

Fig. 8: HRTEM image of the Pd/In_2O_3 catalyst after reduction at 673 K. The image shows the In_2O_3 substrate, decorated with PdIn nanoparticles. The inset FFT evidences that the bottom nanoparticle is imaged along the [111] zone axis. The black arrows indicate the layer covering the entire surface of the nanoparticles. When crystalline the layer spacing is approximately 2.5Å.

a slower rate compared to after pre-reduction at 473 K. Above 570 K, the reaction rates are comparable. XRD measurements at this reduction stage indicate the formation of bulk Pd-In particles and no signs of metallic Pd being left. TEM images reveal partial encapsulation of some bimetallic particles. Hence, the measured activity again appears to be a superposition of the activities and selectivities of the PdIn bimetallic and In_2O_3. At 673 K pre-reduction temperature, the dominating bulk species is Pd_2In_3 according to XRD. However, since TEM images reveal that an increasing number of bimetallic particles are encapsulated by In_2O_3, we expect a decreasing contribution from the bimetallic and a selectivity pattern that more closely resembles In_2O_3. Indeed, after pre-reduction at 673 K, the onset temperature is shifted to 550 K and the activity/selectivity pattern is typical for pure In_2O_3. In all cases, at maximum 5-6% CO (at 673 K reaction temperature) has been observed in the product mixture. The H_2 traces are not shown for the sake of clarity but CO_2 and hydrogen are produced in a 1:3 molar ration, in agreement with the stoichiometry of the methanol steam reforming reaction. For comparison, the corresponding methanol steam reforming reaction over pure In_2O_3 powder, after an oxidation-reduction cycle at 673 K and 573 K, respectively, is also shown in the left panel. It is immediately obvious, that the onset of reaction is around 560 K, close to the reaction onset temperature over the Pd/In_2O_3 catalyst pre-reduced at 673 K. This again confirms the encapsulation of bimetallic particles by In_2O_3, as verified by TEM, shown in Figure 8.

The right panel of Figure 9 (b and d) shows the corresponding experiments on the thin film after pre-reduction at 373 K and 573 K. It is worth to note, that an oxidation treatment at 673 K has been performed prior to each reduction. TEM investigations showed Pd metal along with crystallizine bcc-In_2O_3 after this oxidation-reduction treatment at 673 K and 373 K, respectively. The selectivity/activity pattern, nevertheless, is typical for pure In_2O_3 and no methanol dehydrogenation has been observed. Therefore, these results strongly suggest the formation of an In_2O_3 shell surrounding all Pd particles. If the catalyst is reduced at 573 K after the oxidation treatment, TEM indicates formation of a PdIn bimetallic phase, without any signs of Pd being left. However, even in this case, as shown above, only the activity and selectivity of In_2O_3 is measured, which suggests that the In_2O_3 shell is still partially present. It is worth noting, that no other reaction by-products, such as formic acid or the like are present in detectable concentrations. Similarly to Pd/Ga_2O_3, a low-temperature decarboxylation pathway of formic acid must hence be prevalent on the active and selective state of the catalyst [7].

In a similar argumentation outlined for pure In_2O_3, Ga_2O_3 and Pd/Ga_2O_3, respectively, the turnover frequencies and apparent activation energies over the PdIn/In_2O_3 powder catalyst can be determined. For the state after reduction at 573 K, the number of active catalytic sites and thus, the turnover frequencies, were calculated as follows: from a sample mass of 0.011 g, the mass of Pd was determined as 0.00132 g, according to 12% Pd/In_2O_3. Considering a mean particle diameter from TEM of 7.5 x 10^{-9} m after reduction at 573 K and assuming hemispherical particles, the number of Pd particles, on the basis of the Pd mass, was determined to be $4.2x10^{14}$. This yields a Pd surface of the catalyst of 0.0658 m^2. The total number of metal surface sites finally results in 1.24 µmol (the space required for one Pd atom was determined to be 8.8 x 10^{-20} m^2 assuming an isotropic contribution from (111), (100) and (110) facets). From the initial CO_2 slopes of methanol steam reforming reactions at 513 K, 543 K and 573 K and the number of active sites the turnover frequencies based on CO_2 formation were determined to be 0.4 h^{-1} (513 K), 1.6 h^{-1} (543 K) and 1.9 h^{-1} (573K). A corresponding Arrhenius plot ln(TOF) versus reciprocal reaction temperature results in an apparent activation energy of ~ 64 kJ mol^{-1}, which is comparable to Pd/Ga_2O_3 [7], but considerably less than for clean In_2O_3 (~100 kJ mol^{-1}) [4].

4. Conclusions

Despite the striking similarities of Pd supported on ZnO, Ga_2O_3 and In_2O_3 regarding bimetallic formation at comparatively low substrate temperatures and catalytic selectivity in methanol steam reforming, the structural complexity (and, in turn, also their influence on catalytic properties) increases from ZnO over Ga_2O_3 to In_2O_3. Concerning the use of thin film model systems, this essentially refers to the crystallinity of the supporting oxide and its easy reducibility. ZnO and Ga_2O_3 are both amorphous in their respective as-grown states [7,11], thereby facilitating the discrimination of the Pd particles from the supporting material. In contrast, Pd particles are almost invisible in the

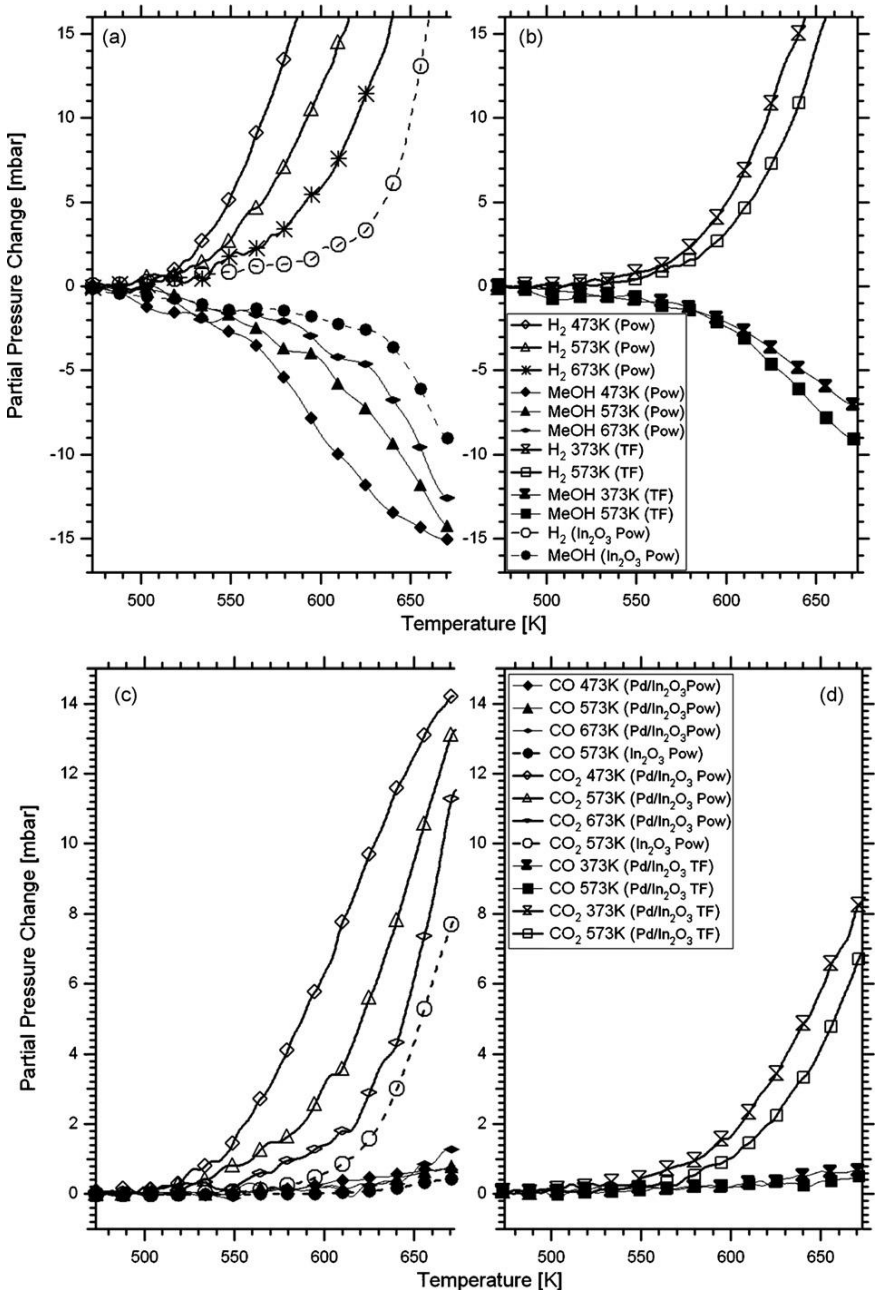

Fig. 9: Temperature-programmed methanol steam reforming reaction on the Pd/In_2O_3 powder samples after reduction at 473 K, 573 K and 673 K (left panel; a-H_2 and methanol traces; c-CO/CO_2 traces) and on the Pd/In_2O_3 thin film sample after reduction at 373 K and 573 K (right panel; b-H_2 and methanol traces; d-CO/CO_2 traces). For comparison, the corresponding reaction over pure In_2O_3 powder (dotted lines), after a similar treatment, is also shown in the left panel. Sample mass of the powder catalyst: 50.0 mg; Pre-oxidation of all catalysts at 673 K in 1 bar O_2 for 1h before reduction. Reduction in 1 bar H_2 was performed for 1 h each. Heating ramp: 5 K/min

as-deposited state if embedded in In_2O_3. As the reducibility of the oxides increases from ZnO to In_2O_3, In metal formation during the deposition process of In_2O_3 may lead to Pd-In bimetallic formation already at low substrate temperatures. This is unique among the three oxides studied. Hence, oxidative treatments lead to decomposition of the PdIn bimetallic and the formation of an In_2O_3 shell around the Pd particles which prevents proper catalytic characterization of the PdIn bimetallic. This phenomenon has also been observed for Pd/Ga_2O_3, but only after reduction at higher temperatures ($T \geq 673$ K) and subsequent oxidation at 673 K [7]. The activity and selectivity of the Pd-In bimetallic could only be studied on the respective powder samples, where the high CO_2 selectivity of the PdIn phase in contact with the oxide could be verified. The catalytic contribution of the oxide-supported Pd_2In_3 phase could not be properly assessed because of strong metal-support interaction effects leading to encapsulation of the bimetallic particles by crystalline In_2O_3. None of these effects have

been observed for the corresponding ZnO and Ga_2O_3-based powder systems.

In conclusion, Pd/In_2O_3 is the most complex of the three systems studied from both a structural and a catalytic point of view.

Acknowledgements

We thank the Austrian Science Foundation for financial support under project P-20892-N19. The authors acknowledge support from the European Union under the Framework 6 program under a contract from an Integrated Infrastructure Initiative (Reference 026019 ESTEEM).

References

[1] T. Hirano, Y. Ozawa, T. Sekido, T. Ogino, T. Miyao, S. Naito, Appl.Catal. A 320 (2007) 91-97
[2] F. A. Marchesini, S. Irusta, C. Querini, E. Miro, Appl. Catal. A 348 (2008) 60-70
[3] N. Iwasa, T. Mayanagi, N. Ogawa, K. Sakata, N. Takezawa, Catal. Lett. 54 (1998) 119-123
[4] H. Lorenz, W. Jochum, B. Klötzer, M. Stöger-Pollach, S. Schwarz, K. Pfaller, S. Penner, Appl. Catal. A 347 (2008) 34-42
[5] J. M. Tatibouet, Appl. Catal. A 148 (1997) 213-252
[6] Landolt-Börnstein, Phase Equilibria, Crystallographic and Thermodynamic Data of Binary Alloys, New Series IV/5G, p. 142, Springer, Heidelberg 1997
[7] S. Penner, H. Lorenz, W. Jochum, M. Stöger-Pollach, D. Wang, C. Rameshan, B. Klötzer, Appl. Catal. A 358 (2009) 193-202
[8] H. Lorenz, S. Penner, W. Jochum, C. Rameshan, B. Klötzer, Appl. Catal. A 358 (2009) 203-210
[9] G. Rupprechter, K. Hayek, H. Hofmeister, J. Catal. 173 (1998) 409-422
[10] C. Zimmermann, K. Hayek, Chem. Ing. Technol. 63 (1991) 68-71
[11] S. Penner, B. Jenewein, H. Gabasch, B. Klötzer, D. Wang, A. Knop-Gericke, R. Schlögl, K. Hayek, J. Catal. 241 (2006) 14-19
[12] H. Lorenz, M. Stöger-Pollach, S. Schwarz, K. Pfaller, B. Klötzer, J. Bernardi, S. Penner, J. Phys. Chem. C 112 (2008) 918-925
[13] M. Nakamura, N. Kimizuka, T. Mohri, M. Isobe, J. Solid State Chem. 105 (1993) 535-549
[14] I. R. Harris, M. Norman, A. W. Bryant, J. Less-Common Met. 16 (1968) 427-440
[15] T. Skala, K. Veltruska, M. Moroseac, I. Matolinova, G. Korotschenkov, V. Matolin, Appl. Surf. Sci. 205 (2003) 196-205
[16] J. B. Darby Jr., K. M. Myles, J. N. Pratt, Acta Metall. 19 (1971) 7-14
[17] H. J. Schaller, H. Brodowsky, Ber. Bunsenges. Phys. Chem. 82 (1978) 773-778
[18] S. Penner, D. Wang, B. Jenewein, H. Gabasch, B. Klötzer, A. Knop-Gericke, R. Schlögl, K. Hayek, J. Chem. Phys. 125 (2006) 094703-1 - 094703-8
[19] E. Hellner, F. Laves, Z. Naturforsch. A 2 (1947) 177-183
[20] N. Ridley, J. Less-Common Metals, 8 (1965) 354-357